Electronic Supplementary Material (ESI) for Materials Chemistry Frontiers.

Supporting Information

Suppression and Utilization of Kasha's Rule: Realizing the transformation from Blue to Near-infrared Emission

Mingchen Xie,[a‡] Jiaheng Cai,[b‡] Guangyu Zhang,[c] Sinyeong Jung,[a] Dongfang Dong,[a] Zhao-yang Zhang,[a] Dongying Zhou,[b]* Liang-sheng Liao,[b] Tao Li[a]*

Table of Contents

Materials and Instruments

The component mentioned in the article are obtained from commercial approach and are dried by vacuum desiccator. ^{1}H NMR spectra are collected by the Bruker 400 AVANCE III HD spectrometer. Molecular masses are determined by Bruker Matrix-Assisted Laser Desorption/Ionization Time of Flight Mass Spectrometry (Bruker-MALDI-TOF-MS). Absorption and photoluminescence (PL) emission spectra of the target compound are measured using a SHIMADZU UV-2700 spectrophotometer and Edinburgh FLS1000 spectrophotometer, respectively. Thermogravimetric analysis (TGA) and differential scanning calorimetry (DSC) are performed on TA-Discovery TGA-550 thermal analyzers and PerkinElmer-DSC 8000 under nitrogen atmosphere at the heating rate of 10 °C min-1. Cyclic voltammetry (CV) measurements are performed on a CHI604E electrochemical workstation, equipped with a three-electrode cell consisting of samples coated on the surface of platinum electrode as working electrode, Ag/Ag+ as reference electrode and a platinum sheet counter electrode. CV measurements are carried out in anhydrous dichloromethane containing 0.1 M n-Bu4NPF6 as electrolyte under an argon atmosphere at a scan rate of 100 mV s-1 assuming that the absolute energy level of Fc/Fc+ is -4.80 eV as standard. The time decay spectra are measured using Variable Pulse Laser (VPL) lamp for 300 ns pulse width - 80 µs lifetime and a microsecond pulsed Xenon light source for 1 µs-10 s lifetime measurement. The synchronization photomultiplier for signal collection and the Multi-Channel Scaling Mode of the PCS900 fast counter PC plug-in card for data processing. Lifetime values are simulated by single exponential fitting function in Fluoracle software.

Partial characterizations have been mentioned in previous work, and we refer those data in this article for readability.

Device fabrication and evaluations

Devices are fabricated on patterned ITO glass substrates with a sheet resistance of 15 Ω per square. Before device fabrication, ITO substrates are cleaned with ethanol, acetone, and deionized water, dried in an oven at 120 °C for 2 h, then treated with UV-ozone for 15 min, and finally loaded into a deposition chamber with a basic pressure of 4×10^{-6} Torr. The device structure is ITO/MoO_3 (3 nm)/TAPC (35 nm)/TCTA (10 nm)/CBP: x wt%/B3PYMPM (60 nm)/Liq (2 nm)/Al (120 nm). Deposition rates and thicknesses of all materials are monitored with oscillating quartz crystals. The deposited rates for organic materials, Liq, and Al are controlled at 1^{-2}, 0.1, and 5 Å s^{-1}, respectively. The Electroluminescence spectra and current density-voltage (L-J-V) characteristics of the devices are measured using a constant current source (Keithley 2400 SourceMeter) combined with a photometer (Photo Research SpectraScan PR 655).

Synthetic Procedures[5]

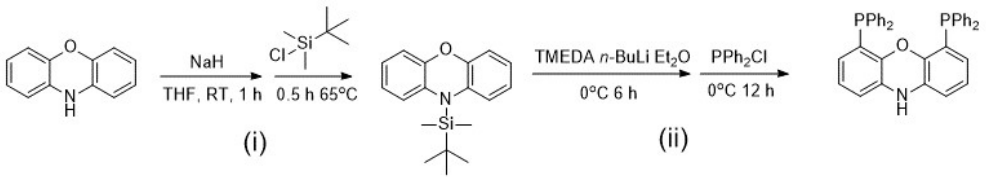

Syntheses of 4,5-bis(diphenylphosphanyl)-10H-phenoxazine (DPh_2P-POZ)

(i) Sodium hydride (0.82 g, ~17.3 mmol) and phenoxazine (2.5 g, 13.65 mmol) was dissolved in anhydrous THF (50 mL) under the N_2 atmosphere and stirred 1 hour at room temperature. The tert-butyldimethylchlorosilane (3.0 g, ~20 mmol) which dissolved in a DMF-THF mixture (1:4,10 mL) was added thereinto. The reaction was slowly heated to 65°C and maintained about half hour. Then it can be quenched by water and extracted via DCM. The 10-(*t*Butyldimethylsilyl)phenoxazine (**1**) was purified by recrystallization (DCM/PE) and proceed to the next step. (ii) the TMEDA (3 mL, ~20 mmol) and **1** (2.38 g, 8 mmol) was dissolved in 100 mL diethyl ether (Et_2O) at 0 °C under the N_2 atmosphere. The 2.5 M n-butyllithium (8.1 mL, 20 mmol,) was dropped into the solution and stirred 6 hours at 0 °C. Then the chlorodiphenylphosphine (3.6 mL, 20 mmol, diluted by 5 mL Et2O) was dropped into the reaction. After stirring 12 hours, the reaction was quenched by water and extracted by DCM. After removing the solvent, the residue was dissolved in 50 mL THF and tetrabutylammonium fluoride trihydrate (4.3 g, 13.7 mmol) was added with stirring for 5 hours at 50 °C to detach the *t*Butyldimethylsilyl. Finally, after extracting by DCM, the organic layer was removed and recrystallized via DCM/MeOH. About 3.0 g reseda powder, yield: ~69%.

^{1}H NMR (400 MHz, CDCl3): δ = 7.46-7.02 (m, 20 H), 6.64 (t, *J* = 8.0, 16.0 Hz, 2 H), 6.38 (d, *J* = 8.0 Hz, 2 H), 6.03 (d, *J* = 8 Hz, 2 H), 5.21 (s, 1 H).

Syntheses of 2,6-bis(4,5-bis(diphenylphosphanyl)-10H-phenoxazin-10-yl)phenazine (DPh_2P-POZ-PZ)

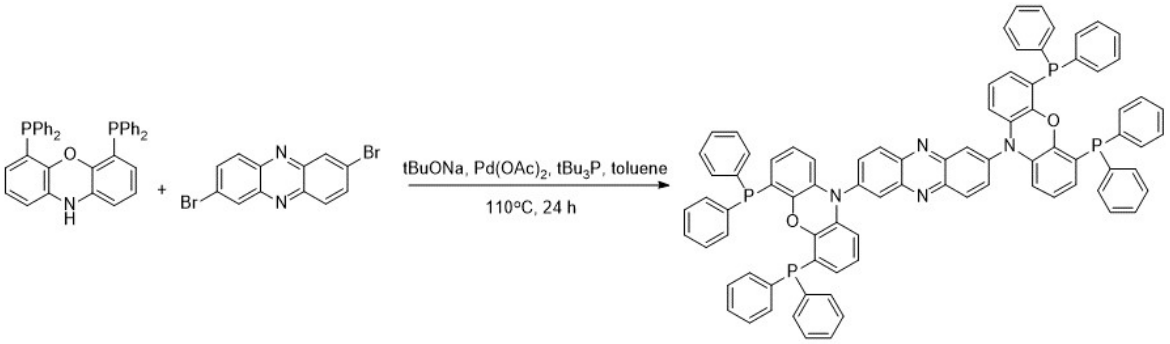

2,6-DBr-PZ (1.01 g, 3 mmol), DPh_2P-POZ (3.36 g, 6.1 mmol), *t*-BuONa (0.58 g, 6.1 mmol) and $Pd(OAc)_2$ (0.007 g, 0.03mmol) were added into 25 mL toluene, followed by tBu_3P (0.006g, 0.03mmol) was added via injector. The mixture solution was refluxed under N_2 atmosphere for 24 h. After cooling to room temperature, the reaction was washed by water and extract via dichloromethane. Solvent of combined organic layers were removed and Residue was purified by column chromatography on silica gel using CH_2Cl_2/hexane (1:1, v/v) as eluent. The puce powder can be further purified via recrystallization using chloroform and ethyl acetate. ~ 2.7 g, final yield ~70.4%.

^{1}H NMR (400 MHz, $CDCl_3$): δ = 8.49 (d, *J* = 8.0 Hz, 2 H), 8.38 (s, 2H), 7.90 (d, *J* = 8.0 Hz, 2 H), 7.47-7.08 (m, 40 H), 6.56 (t, *J* = 8.0, 16.0 Hz, 4 H), 6.19 (d, *J* = 8.0 Hz, 4 H), 6.14 (d, *J* = 8.0 Hz, 4 H). MALDI-TOF MS (mass m/z): 1279.244 $[M]^+$, calculated for $C_{84}H_{58}N_4O_2P_4$: 1279.31.

DFT calculations

The ground state optimization is performed using popular 6-31G** basis and B3LYP function. All structures are further verified by harmonic vibrational frequency analysis to ensure that real local minima had been found without imaginary vibrational frequency. All ground state structures are adjusted by dispersion correction. The excited state is simulated at TD-B3LYP-6-31** level. Multifwn[3] and VMD are employed to perform the excited states analysis. The total energies are also corrected by zero-point energy both for the ground state. All computations are performed using the Gaussian 09 package[2]

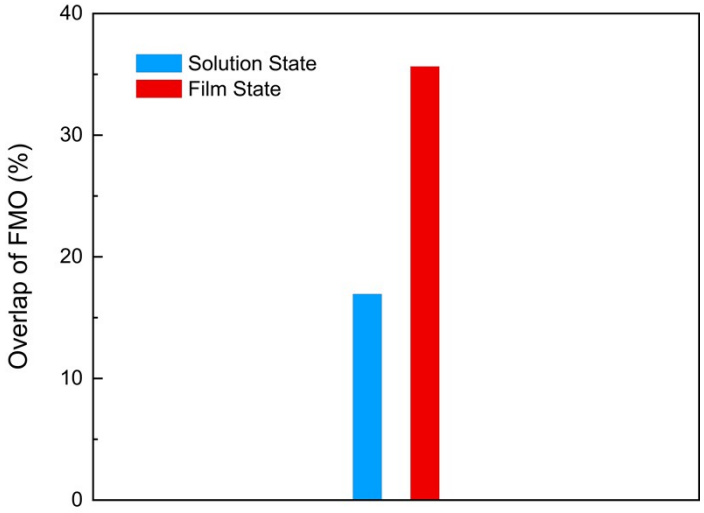

Figure S1. The overlap of HOMO and LUMO for solution state and film state.

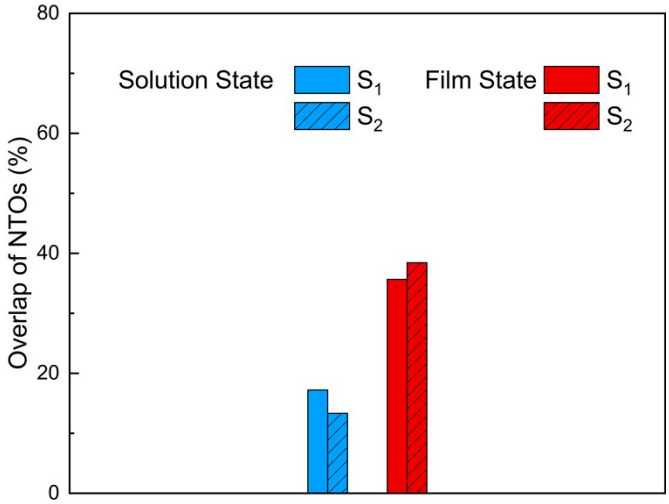

Figure S2. The overlap of NTO in solution state and film state.

The figure 1 and figure 2 are the overlaps of FMO and NTO, respectively. For NTOs, the POZ-PZ has relatively small overlap due to the large dihedral angle. The overlaps for vertical configuration (solution state) are 17.21% for S_1 and 13.32% for S_2, respectively. Depending on the locations of hole and particle, the POZ-PZ is representative charge-transition (CT) type excited state. Meanwhile, the overlaps of film state are remarkably increasing, which is 35.65% for S_1 and 38.44% for S_2, respectively. Importantly, the excited state of film state still is CT-type. As mentioned in straight matter, CT-type excited state is effortlessly affected by the molecular configuration. Therefore, the different emission could be attributed to the variable molecular configurations which correspond with the variable excited state.

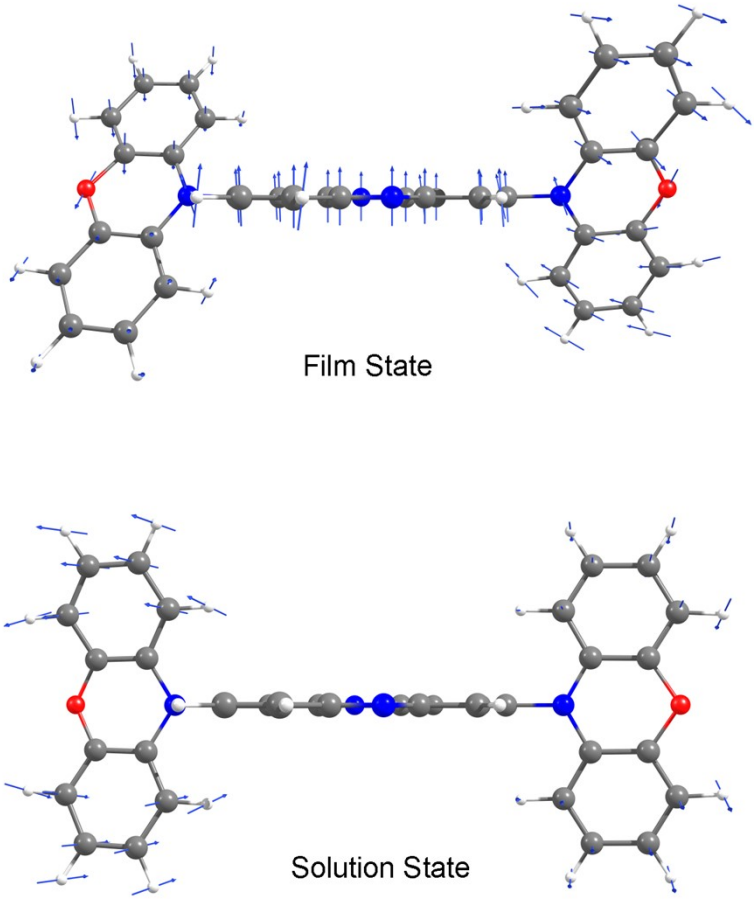

Figure S3. The vibration vector of POZ-PZ in different matrixes.

Regarding POZ-PZ, if electrons can effectively transfer to PZ, the vibration of the PZ group will be strong, indicating that the PZ group is more involved in electronic interactions. Therefore, the vibration vector is analyzed to qualitatively illustrate the degree of acceptor involvement. As shown in Figure S3, the vibration vector analysis in the film state reveals that the POZ group undergoes reciprocatedly twisting vibrations around the N-O axis; the N and O atoms exhibit opposite twisting modes; and the PZ group performs scissoring vibrations due to efficient charge transfer. In the solution state, the outer four carbon atoms of the POZ group perform twisting vibrations, while the middle four carbon atoms and the N and O atoms do not vibrate, and the PZ group has no vibration vector. This indicates that when the dihedral angle is vertical in the solution, electrons cannot effectively transfer to the PZ group. In this case, the molecule undergoes reciprocatedly twisting vibrations around the N-O axis for relaxation, which may be the main source of blue emission. When the POZ group undergoes reciprocal twisting to bring the dihedral angle below 90°, electrons can transfer to the PZ group, resulting in near-infrared emission for the molecule. In the film state, the dihedral angle of the molecule is induced and constrained by the rigid matrix to be 68.9°, and the POZ group does not twist. In this state, electrons can efficiently transfer from POZ to PZ, resulting in a significant vibration vector on the group, further exhibiting NIR emission.

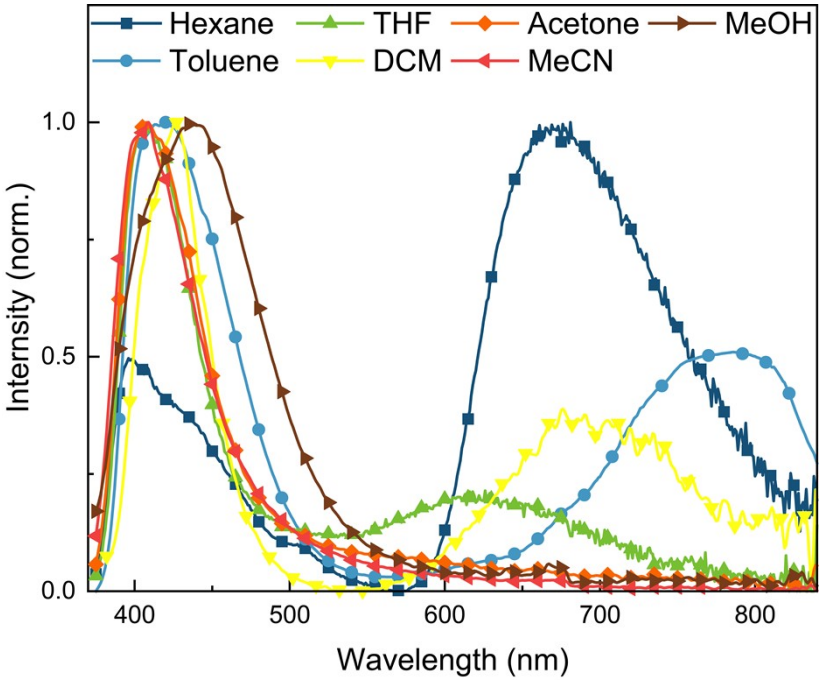

Figure S4. Photoluminescence spectra of POZ-PZ in different solutions (10^{-5} mol L^{-1}); tetrahydrofuran (THF); dichloromethane (DCM); methyl alcohol (MeOH); acetonitrile (MeCN).

The solvent-dependent photoluminescence spectra of POZ-PZ are shown in this section to prove the characteristics excited state. As we mentioned in text, the fundamental of TD-DFT is Born-Oppenheimer approximation. Depending on the Born-Oppenheimer approximation, the mass of the nucleus is 3-4 orders of magnitude larger than that of the electron, generally. Therefore, under the same interaction, the electron will move much faster than the nucleus. The moment seems to be moving in the potential field which is composed by stationary atomic nuclei, and the atomic nucleus would not be affected by the specific position of the electron, but can only be subjected to the average force. In this way, this approximate variables of nuclear coordinates and electron coordinates can be separated, and the complex process of solving the wavefunction of the whole system can be decomposed into two relatively simple processes: solving the electron wavefunction and solving the nuclear wavefunction. However, the blue emission of POZ-PZ is attributed to the self-vibration process. The time-range of vibration relaxation is about 10^{-14}~10^{-12} second, which prominently faster than the radiative transition of singlet state (10^{-8} s). Hence the TD-DFT cannot catch the real surfaces of excited state to solve the Schrodinger equation utilizing the Born-Oppenheimer approximation. Although the blue emission generated from S_2 can be detected, the real motion of electrons moving along with the nucleus still is very difficult to illustrate.

Despite difficult to illustrate by TD-DFT, however, the solvent-dependent photoluminescence spectra could explain the self-vibration process well. As shown in figure S4, all solvents are unrestricted and all photoluminescence curves have two emission band. As mentioned in text, the long-wavelength bands are attributed to the CT-type excited state. Therefore, the emission peak would conspicuously change following with the variation of solvent polarity. Contrarily, the short-wavelength peak ascribes to the self-vibration of POZ group, which means that the excited state is local excitation. Importantly, the experimental results sufficiently show evidence for our viewpoint: short-wavelength peaks in different solvents perform a series of negligible shifts, even in methyl alcohol (37 nm bathochromic shift comparing with the Hexane). Therefore, the electron distributions of S_2 obtained from simulation only could be used as quantitative analysis.

Photophysical Properties

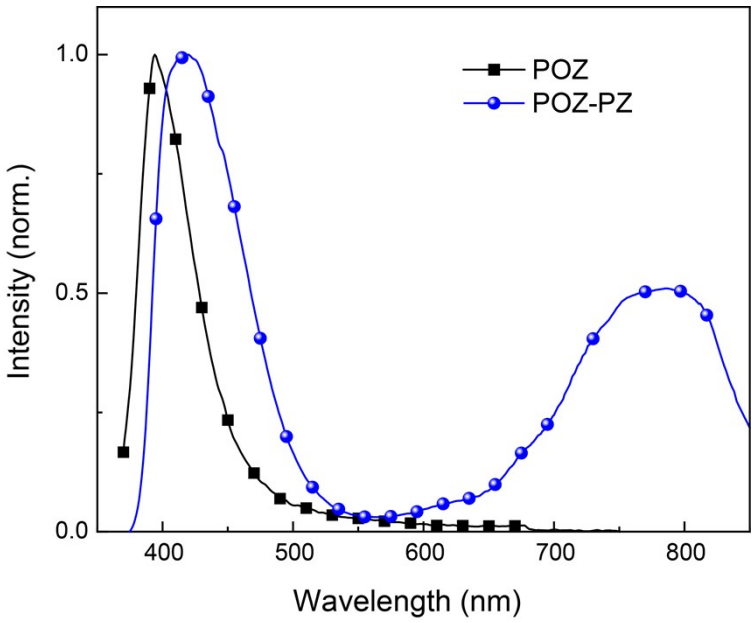

Figure S5. The emission spectra of POZ-PZ and POZ.

The figure S5 shows the PL spectra of POZ and POZ-PZ. The distinct emission difference indicates that the blue emission is from the POZ-PZ group, rather than the POZ group.

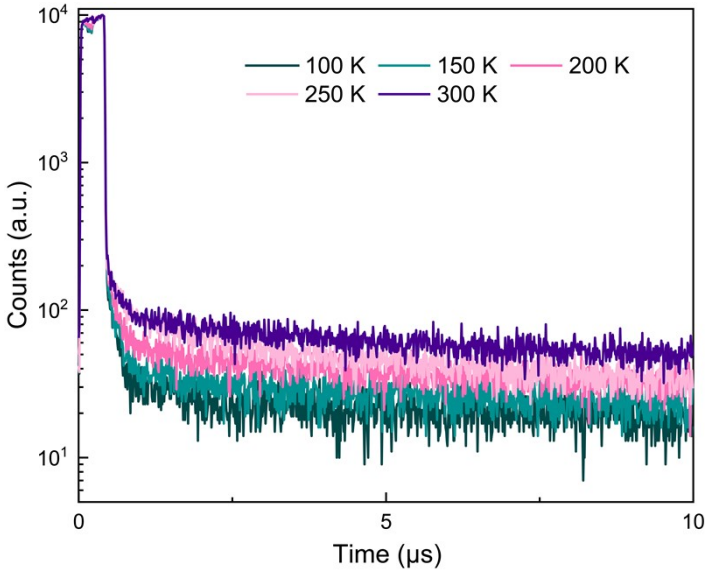

Figure S6. The temperature-dependent transient PL (100–300 K) decay curves of POZ-PZ in PMMA (10 wt% doped film, excitation wavelength: 365 nm).

The figure S6 shows temperature-dependent transient PL (100–300 K) decay curves of POZ-PZ in PMMA film. It clearly demonstrates that the component of delayed fluorescence rapidly increases as the rising of temperature. This process indicates that the POZ-PZ is TADF-type compound.

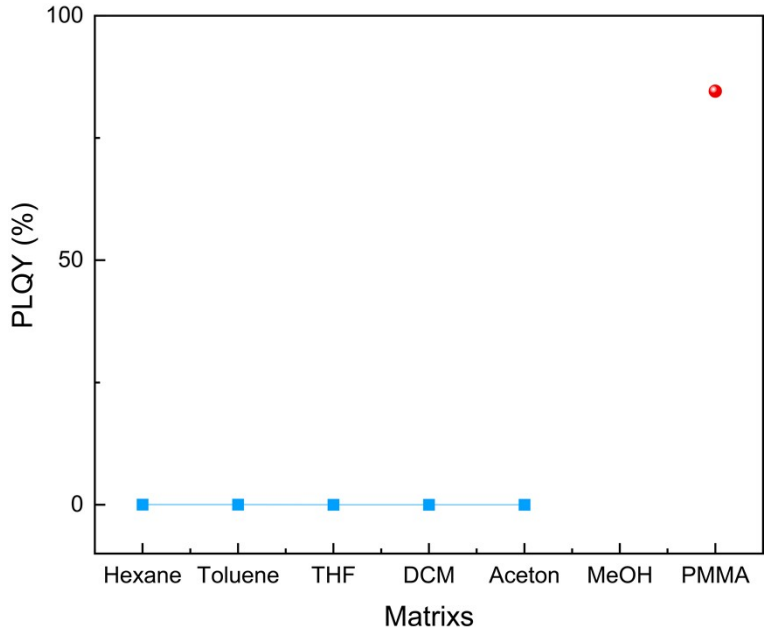

Figure S7. The PLQYs in different matrixes.

Table S1. The summary of PLQY in different solution (10^{-5} mol L^{-1})

	Hexane	Toluene	THF	DCM	Aceton	MeOH	PMMA
POZ-PZ	1.59%	1.50%	0.31%	0.48%	~0.10%	Na (quenched)	84.57%

Figure S7 is the PLQY of POZ-PZ in different solutions and 10% PMMA film. The polarity of solutions is incremental. The detailed quantum yields are recorded in Table S1. As mentioned in text, due to the non-radiative transition, the PLQY in solution is very low (blue block). However, the PLQY strongly increases in the rigid matrix (red dot). Meanwhile, the emission change from blue to NIR. In the previous work, we obtained a very low PLQY in the spin CBP film, which results from the difference of crystallinity between the host and guest. Contrarily, PMMA is polymer, which could effectively circumvent the damage resulting from the difference of crystallinity. Therefore, the PLQY in PMMA is relatively higher than that in CBP with same spin craft.

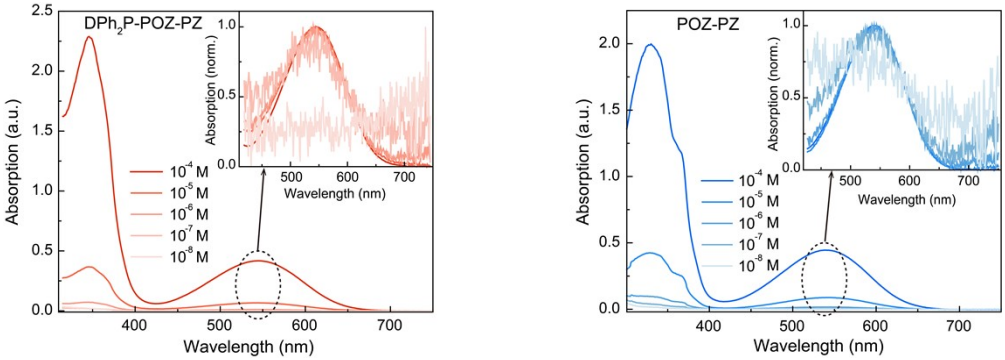

Figure S8. The absorption spectra of DPh_2P-POZ-PZ and POZ-PZ with different concentration gradient.

With the consideration about dimer or aggregation formed in solution, especially, about the absorption band around 550 nm, we tested a series of absorption spectra with different concentration to ensure that no band is composed by the dimer or aggregation. As shown in figure S8, the testing concentration is from 10^{-4} M to 10^{-8}. The results show that the absorption band around 533 nm always exists in the spectra from the concentration of 10^{-4} M to that of 10^{-7} M, although the 10^{-7} M has been in the critical point of LOD (10^{-8} M exceeds the LOD of instrument). In fact, the absorption band around 533 nm is the characteristic absorption band of POZ-PZ molecule, rather than the band of dimer (or aggregation). This characteristic band also appears in the absorption spectra of DPh_2P-POZ-PZ, and we also tested it with different concentration. The results also prove that the band around 550 nm is not formed from the dimer or aggregation.

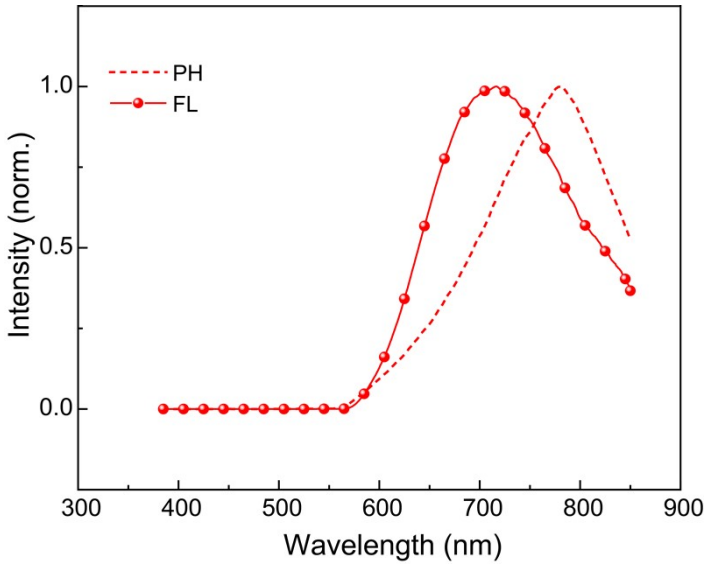

Figure S9. The phosphorescence spectrum of POZ-PZ in 10% PMMA film at room-temperature.

According to the PH and FL spectra of POZ-PZ in PMMA film, the splitting energy (ΔE_{ST}) could be estimated, which is about 0.14 eV (difference value between the FL peak energy and PH peak energy). This value is distinctly smaller than the threshold value (0.3 eV normally).

TADF Parameters Estimation.

The key rate constants of TADF process were calculated based on the following equations[4]:

$$k_{PF} = \frac{\phi_{PF}}{\tau_{PF}} \quad (1)$$

$$k_{DF} = \frac{\phi_{DF}}{\tau_{DF}} \quad (2)$$

$$k_{ISC} = \frac{\phi_{DF}}{\phi_{DF} + \phi_{PF}} \cdot k_{PF} \quad (3)$$

$$k_{RISC} = \frac{k_{DF} k_{PF}}{k_{ISC}} \cdot \frac{\phi_{DF}}{\phi_{PF}} \quad (4)$$

Table S2. Summary of photophysical properties of POZ-PZ in different matrixes

	FL.	Lifetime (ns)	Lifetime[a] (μs)	Φ_{total}	Φ_{PF}[b]	Φ_{DF}[b]	k_{RISC} (10^5 s^{-1})
Toluene	420,780	3.40/8.71	11.90/2.40	1.50	0.44	1.06	30.0/0.15
10% PMMA film	715	90.81	1.84	84.57	8.87	75.70	39.0

[a] The blue emission is measured in the solution state (10^{-5} mol L^{-1})/the NIR emission is measured in the solution state (10^{5} mol L^{-1}). [b] Φ_{prompt} and $\Phi_{delayed}$ are determined by using total PL quantum efficiency and the ratio between prompt and delayed components which is calculated from transient PL measurement.[1]

The table S2 is the summary of photophysical properties. It is worth noting that the blue emission in toluene solution has a very fast reverse intersystem crossing rate (k_{RISC}), however, regarding NIR emission, the k_{RISC} is very small. In consideration of the intramolecular motions, the small k_{RISC} of NIR primarily results from the spin-forbidden transition (or we could say low charge transition efficiency) between the donor and acceptor. Meanwhile, the strong non-radiative transition enormously lowers the PLQY in toluene solution. Comparing with the NIR emission, the k_{RISC} of blue emission is relatively large. Obviously, in the unrestricted solution, the self-vibration which forms the blue emission does not be dominated by the charge transition, therefore having large k_{RISC}. On the other hand, contrasting the k_{RISC} of NIR emission in different matrixes, a distinct increase for k_{RISC} could be found, which is resulting from the effective charge transition formed in restricted matrixes.

Table S3. Summary of photophysical properties for POZ-PZ and DPh_2P-POZ-PZ.

	Emission (Sol.)	Emission (PMMA)	Emission (Thin film)	Emission (Freezing)	PLQY (PMMA)	PLQY (Sol.)
POZ-PZ	420/780 nm	715 nm	760 nm	725 nm	84.57%	1.50%
DPh_2P-POZ-PZ	758 nm	703 nm	744 nm	677 nm	3.93%	0.5%

Thermodynamic Properties

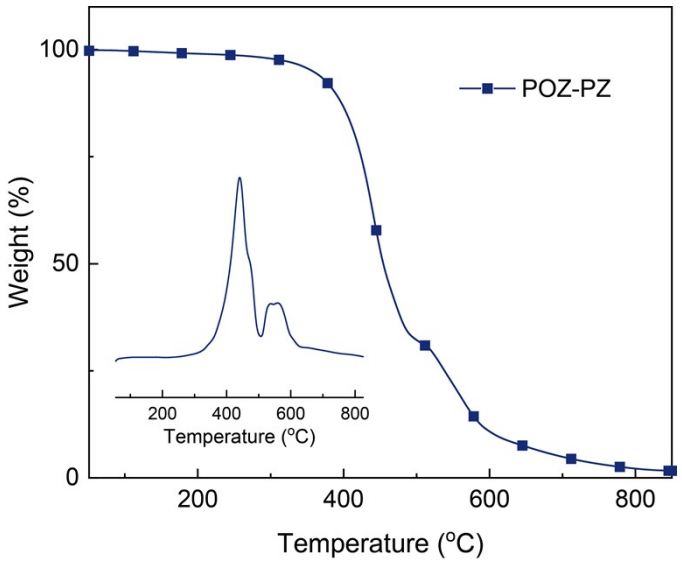

Figure S10. The TGA and DSC curve of POZ-PZ.

Table S4. Summary of TGA and DSC.

	T_g (°C)	T_d (°C)
POZ-PZ	371	271

Electrical Properties

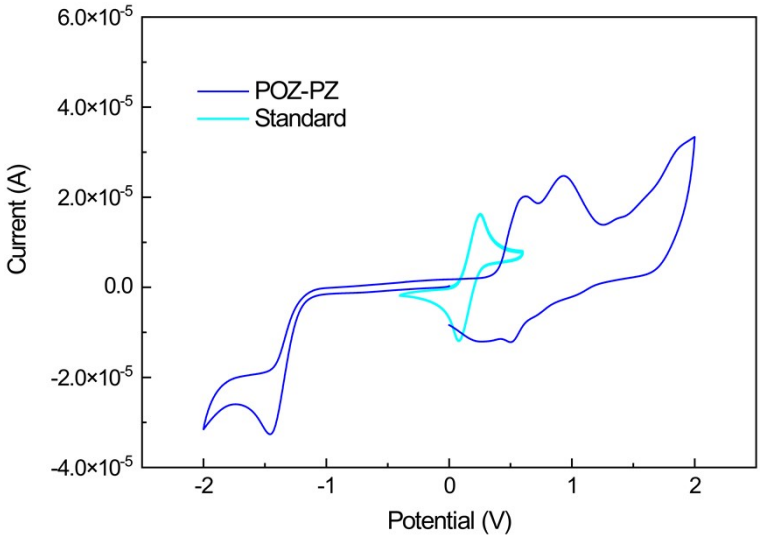

Figure S11. The cyclic voltammogram curves of POZ-PZ and ferrocene.

Structural characterization

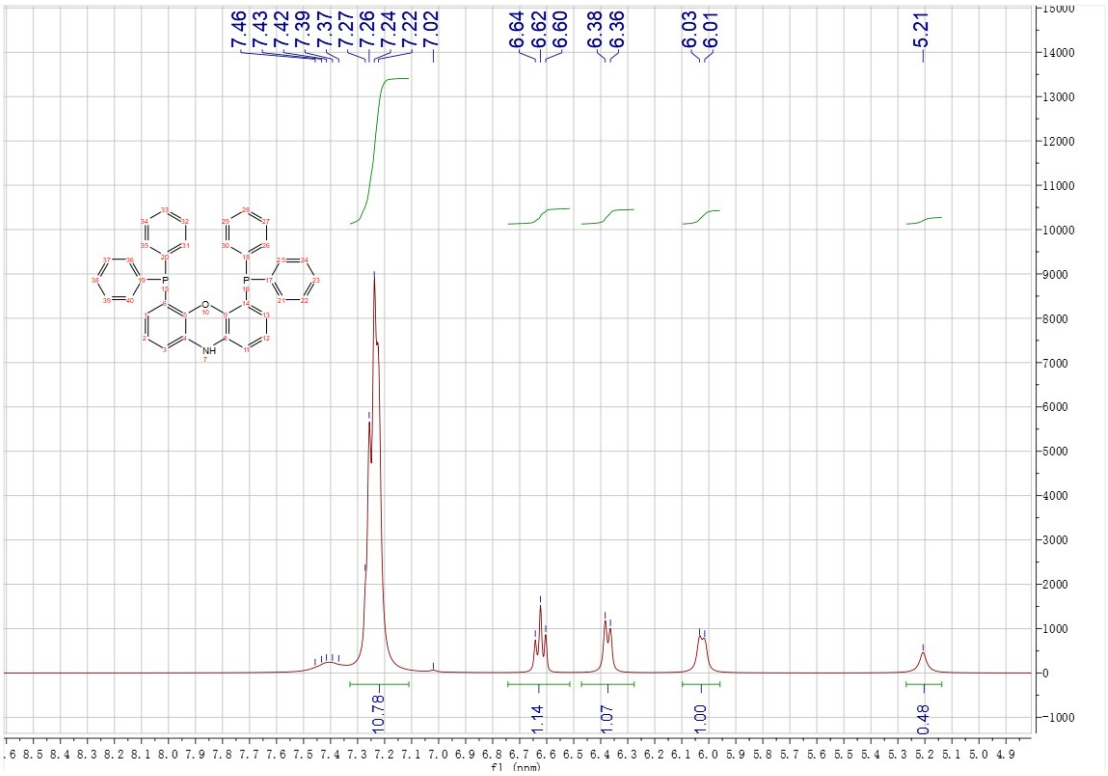

Figure 12. ^{1}H NMR (400 MHz, $CDCl_3$) of DPh_2P-POZ.

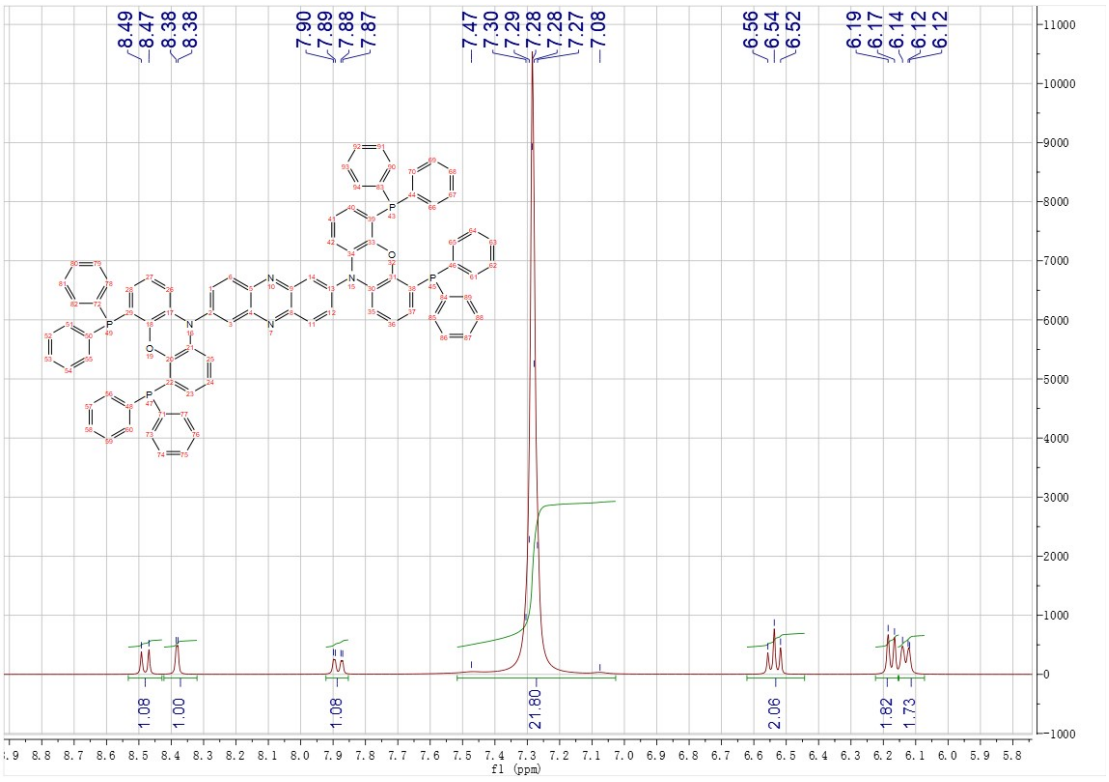

Figure S13. ^{1}H NMR (400 MHz, $CDCl_3$) of DPh_2P-POZ-PZ.

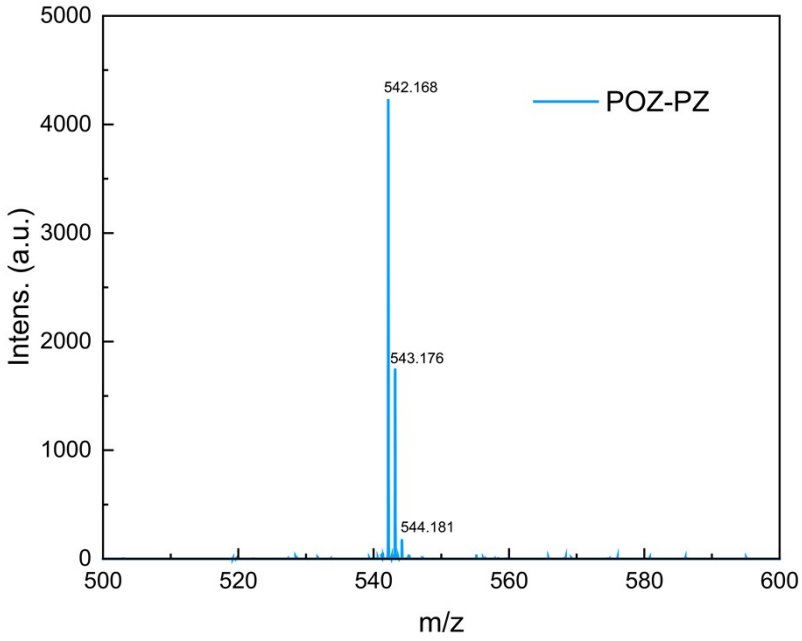

Figure S14. MODI-TOF-MS of POZ-PZ.

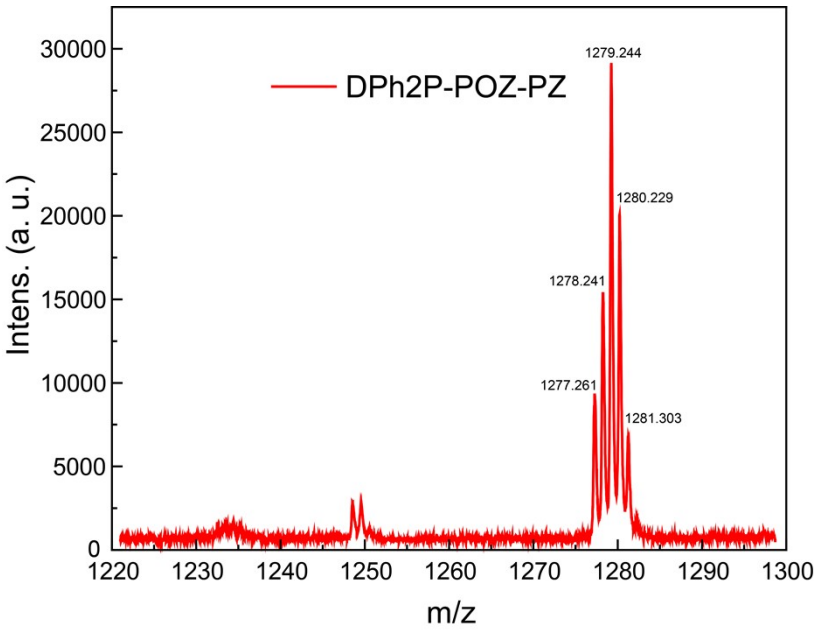

Figure S15. MODI-TOF-MS of DPh_2P-POZ-PZ.

Simulation data

Although we have tried many times, the crystal of POZ-PZ still cannot be obtained. As far as we can tell, the intense Intramolecular motion is the primary cause of preventing crystallization. However, the MODI-TOF-MS and ^{1}H NMR have already sufficiently proved the accuracy of POZ-PZ. Meanwhile, the crystal only could characterize the morphology of stacking, which could not represent the real configuration of POZ-PZ in solution. Therefore, the feasible structures of POZ-PZ subject to the simulated results.

POZ-PZ (solution state)

0 1

C	3.62803300	0.00000300	-0.23661600
C	2.67814100	0.00000400	0.74858000
C	1.29371300	0.00000400	0.39992500
C	0.91855100	0.00000500	-0.99709700
C	1.94400000	0.00000400	-1.99213100
C	3.26111600	0.00000300	-1.62062600
C	-1.29371300	0.00000400	-0.39992500
C	-0.91855100	0.00000500	0.99709700
C	-1.94400000	0.00000400	1.99213100
H	-1.64269100	0.00000400	3.03444500
C	-3.26111600	0.00000300	1.62062600
C	-3.62803300	0.00000300	0.23661600
C	-2.67814100	0.00000400	-0.74858000
H	2.95744600	0.00000300	1.79648700
H	1.64269100	0.00000400	-3.03444500
H	4.05120600	0.00000200	-2.36451700
H	-4.05120600	0.00000200	2.36451700
H	-2.95744600	0.00000300	-1.79648700
N	-0.36931200	0.00000500	-1.37199700
N	0.36931200	0.00000500	1.37199700
C	-5.73366700	-1.21168500	-0.05708600
C	-5.73367200	1.21168400	-0.05708800
C	-5.11522400	-2.45005900	0.14723200
C	-7.12854200	-1.18315500	-0.23243900
C	-7.12854700	1.18314900	-0.23244100
C	-5.11523300	2.45006100	0.14722800
C	-5.87031600	-3.62779800	0.17079000
H	-4.04074000	-2.49456300	0.27873200
C	-7.88099900	-2.34818500	-0.20119800
C	-7.88100800	2.34817600	-0.20120200
H	-4.04075000	2.49457000	0.27872700
C	-5.87033000	3.62779700	0.17078300
C	-7.25204700	-3.58281200	-0.00175300
H	-5.36610500	-4.57645300	0.32499300
H	-8.95447000	-2.27455900	-0.34157700
C	-7.25206100	3.58280600	-0.00175900
H	-8.95447800	2.27454500	-0.34158100
H	-5.36612300	4.57645400	0.32498500
H	-7.84272200	-4.49272800	0.01557500
H	-7.84274000	4.49271900	0.01556600
C	5.73366700	-1.21168500	0.05708600
C	5.73367200	1.21168400	0.05708800
C	5.11522300	-2.45005900	-0.14723200
C	7.12854200	-1.18315500	0.23243900
C	7.12854700	1.18314900	0.23244100
C	5.11523300	2.45006100	-0.14722800
C	5.87031500	-3.62779800	-0.17079000
H	4.04073900	-2.49456300	-0.27873200
C	7.88099800	-2.34818500	0.20119800
C	7.88100800	2.34817500	0.20120200
H	4.04075000	2.49457000	-0.27872700

C	5.87033000	3.62779700	-0.17078300
C	7.25204600	-3.58281200	0.00175300
H	5.36610400	-4.57645300	-0.32499300
H	8.95446900	-2.27455900	0.34157700
C	7.25206100	3.58280500	0.00175900
H	8.95447900	2.27454400	0.34158100
H	5.36612300	4.57645500	-0.32498400
H	7.84272100	-4.49272900	-0.01557500
H	7.84274100	4.49271900	-0.01556600
N	-5.01481000	0.00000100	-0.11465000
N	5.01481000	0.00000100	0.11465000
O	-7.79804500	-0.00000500	-0.48220600
O	7.79804500	-0.00000500	0.48220600

POZ-PZ (film state)

0 1

C	3.62410900	-0.04619500	-0.34775800
C	2.69598700	-0.05732000	0.66320700
C	1.30428300	-0.04533600	0.35958100
C	0.88309100	-0.05083500	-1.02276800
C	1.87981700	-0.05721500	-2.04600000
C	3.20617400	-0.05230100	-1.71839900
C	-1.30430000	-0.04507900	-0.35902300
C	-0.88310600	-0.05133100	1.02332500
C	-1.87984400	-0.05812100	2.04656300
H	-1.54295100	-0.05385300	3.07725400
C	-3.20619000	-0.05294300	1.71897000
C	-3.62412700	-0.04610700	0.34832500
C	-2.69602400	-0.05678200	-0.66264600
H	2.99552300	-0.07196700	1.70451600
H	1.54293900	-0.05241200	-3.07669400
H	3.97153700	-0.04452500	-2.48661000
H	-3.97158000	-0.04547900	2.48715800
H	-2.99553400	-0.07081700	-1.70397100
N	-0.41306900	-0.04578700	-1.36422400
N	0.41303900	-0.04652900	1.36478800
C	-5.82024400	-1.10662600	0.46267400
C	-5.62826500	1.10429500	-0.53356000
C	-5.27851500	-2.31867200	0.90281000
C	-7.21862600	-0.99289300	0.38336100
C	-7.03255300	1.15304200	-0.59893000
C	-4.91017700	2.19201600	-1.03873600
C	-6.10981000	-3.37011100	1.29609300
H	-4.20271900	-2.43813300	0.93525600
C	-8.04513500	-2.03946500	0.76339200
C	-7.68863100	2.23134000	-1.17384000
H	-3.82989300	2.19073300	-0.97976300
C	-5.57040300	3.28333500	-1.60816200
C	-7.49276500	-3.23413800	1.23252300
H	-5.66359600	-4.29642800	1.64230700
H	-9.11744400	-1.89758500	0.68577100
C	-6.95883300	3.30662100	-1.68461000
H	-8.77263900	2.21267300	-1.19879900
H	-4.98443400	4.11252800	-1.99054300
H	-8.14392100	-4.04716100	1.53475800
H	-7.47682700	4.14870900	-2.13050100
C	5.82012800	-1.10675000	-0.46266100
C	5.62840400	1.10411600	0.53371500
C	5.27826600	-2.31853400	-0.90338700
C	7.21852100	-0.99317900	-0.38339700

C	7.03268800	1.15274500	0.59904100
C	4.91043600	2.19207400	1.03857400
C	6.10942900	-3.36985300	-1.29721700
H	4.20245100	-2.43785600	-0.93582900
C	8.04491100	-2.03963400	-0.76403300
C	7.68889400	2.23119200	1.17354300
H	3.83014800	2.19084400	0.97965800
C	5.57077900	3.28350500	1.60762400
C	7.49241100	-3.23403100	-1.23368000
H	5.66311600	-4.29597100	-1.64383800
H	9.11723600	-1.89786900	-0.68641500
C	6.95922400	3.30669900	1.68399300
H	8.77290100	2.21240900	1.19847700
H	4.98491300	4.11287200	1.98978800
H	8.14346700	-4.04697000	-1.53635000
H	7.47729600	4.14889100	2.12959400
N	-5.01610900	-0.01821800	0.06887100
N	5.01605900	-0.01855500	-0.06821100
O	-7.82869400	0.15568700	-0.07223600
O	7.82876100	0.15504100	0.07288100

POZ-PZ (scan of potential energy)

opt=modredundant b3lyp/6-31g(d,p) em=gd3bj nosymm

0 1

C	3.62905400	-0.00000100	-0.20229000
C	2.66843400	0.00000100	0.77194400
C	1.28725500	0.00000000	0.41224900
C	0.92482900	-0.00000200	-0.98703100
C	1.95970700	-0.00000300	-1.97149600
C	3.27188300	-0.00000300	-1.58908700
C	-1.28725500	-0.00000100	-0.41225000
C	-0.92482900	0.00000100	0.98702900
C	-1.95970700	0.00000300	1.97149500
H	-1.66241900	0.00000400	3.01428100
C	-3.27188300	0.00000200	1.58908500
C	-3.62905400	0.00000000	0.20228900
C	-2.66843400	-0.00000100	-0.77194600
H	2.93550300	0.00000200	1.82209700
H	1.66241900	-0.00000400	-3.01428300
H	4.07074700	-0.00000400	-2.32284200
H	-4.07074600	0.00000300	2.32284100
H	-2.93550300	-0.00000200	-1.82209900
N	-0.35774000	-0.00000200	-1.37954800
N	0.35774000	0.00000200	1.37954700
C	-5.73027500	-1.21255600	-0.08438400
C	-5.73027600	1.21255500	-0.08438600
C	-5.10332900	-2.45002000	0.08132500
C	-7.13014500	-1.18239600	-0.20499700
C	-7.13014500	1.18239500	-0.20499800
C	-5.10333000	2.45002000	0.08132200
C	-5.85441600	-3.62772500	0.12361900
H	-4.02446600	-2.48999800	0.16912700
C	-7.87674700	-2.34949500	-0.15681700
C	-7.87674800	2.34949400	-0.15682000
H	-4.02446600	2.48999800	0.16912300
C	-5.85441700	3.62772500	0.12361400
C	-7.23948800	-3.58302000	0.00493900
H	-5.34392000	-4.57688600	0.24879400
H	-8.95424500	-2.27165400	-0.25182400

C	-7.23948900	3.58301900	0.00493400
H	-8.95424500	2.27165200	-0.25182700
H	-5.34392100	4.57688700	0.24878800
H	-7.82779700	-4.49365900	0.03668800
H	-7.82779800	4.49365800	0.03668300
C	5.73027600	-1.21255500	0.08438400
C	5.73027500	1.21255600	0.08438500
C	5.10333100	-2.45002000	-0.08132500
C	7.13014600	-1.18239400	0.20499900
C	7.13014400	1.18239600	0.20500000
C	5.10332800	2.45002000	-0.08132500
C	5.85441900	-3.62772500	-0.12361700
H	4.02446800	-2.48999900	-0.16912800
C	7.87674800	-2.34949300	0.15682100
C	7.87674600	2.34949500	0.15682200
H	4.02446500	2.48999800	-0.16912800
C	5.85441500	3.62772600	-0.12361600
C	7.23949100	-3.58301800	-0.00493600
H	5.34392300	-4.57688600	-0.24879300
H	8.95424600	-2.27165100	0.25182900
C	7.23948700	3.58302000	-0.00493400
H	8.95424400	2.27165500	0.25183000
H	5.34391900	4.57688600	-0.24879100
H	7.82780000	-4.49365700	-0.03668400
H	7.82779500	4.49365900	-0.03668100
N	-5.01143800	0.00000000	-0.15708500
N	5.01143800	0.00000000	0.15708300
O	-7.81689600	-0.00000100	-0.39787500
O	7.81689500	0.00000100	0.39787800

42 62 1 6 s 18 5.0
21 61 12 13 s 18 5.0

DPh_2P-POZ-PZ-PZ

0 1

C	-3.65611800	-0.42061900	-0.09337300
C	-2.72231700	-0.37774100	0.91208900
C	-1.33279400	-0.34546500	0.59970900
C	-0.91799400	-0.39272200	-0.78365100
C	-1.91954600	-0.46169200	-1.79997900
C	-3.24372200	-0.47344300	-1.46478100
C	1.27187500	-0.31490800	-0.13276000
C	0.85740500	-0.28042700	1.25113400
C	1.85882000	-0.22926900	2.26846400
H	1.52679300	-0.19531300	3.30018300
C	3.18320400	-0.20805600	1.93368800
C	3.59448100	-0.24174100	0.56144800
C	2.66195500	-0.30824400	-0.44341800
H	-3.01275800	-0.37034900	1.95584500
H	-1.58813800	-0.49105700	-2.83202900
H	-4.01365000	-0.51373700	-2.22744800
H	3.95188900	-0.15767100	2.69694800
H	2.95676700	-0.35353900	-1.48517100
N	0.37592000	-0.37167100	-1.13236500
N	-0.43700400	-0.29114700	1.59931600
C	-5.80180300	-1.57344400	-0.13914000
C	-5.69259700	0.65178600	0.83628000
C	-7.19947700	-1.49895800	-0.09516800
C	-5.21004200	-2.79792200	-0.46461300
C	-7.09972000	0.66946100	0.85809800

C	-5.01397200	1.72131000	1.42394100
C	-8.01818300	-2.59321100	-0.37449400
C	-6.01257200	-3.89682400	-0.77566000
H	-4.13088700	-2.88616200	-0.47393800
C	-7.82720400	1.69227200	1.46733300
C	-5.72677900	2.75817200	2.02985600
H	-3.93330300	1.75367200	1.39786500
C	-7.39987900	-3.80215900	-0.73496400
H	-5.54196300	-4.83726000	-1.04377000
C	-7.11485100	2.74637300	2.06237000
H	-5.18015800	3.58095900	2.47927700
H	-8.01244500	-4.66248400	-0.97476900
H	-7.65525400	3.55083000	2.54486300
C	5.80942700	-1.25229400	0.71455000
C	5.56884900	0.91459900	-0.37742300
C	7.20258300	-1.10681100	0.65064000
C	5.29089800	-2.45833800	1.19647600
C	6.96862200	0.98854600	-0.45729100
C	4.82393000	1.96350700	-0.92365000
C	8.08133000	-2.09737000	1.09372700
C	6.15292400	-3.46039000	1.64504900
H	4.21894800	-2.60889100	1.21865300
C	7.63182100	2.03896800	-1.09622200
C	5.46952400	3.03262200	-1.54667500
H	3.74454800	1.94880200	-0.85522500
C	7.53150200	-3.28588700	1.60360800
H	5.73533000	-4.38875400	2.02108800
C	6.85511700	3.07297000	-1.64448300
H	4.87334100	3.84009000	-1.95943000
H	8.19081900	-4.06875800	1.95702000
H	7.34374100	3.90217900	-2.14043600
O	7.77332600	0.03523400	0.13407200
O	-7.82555200	-0.30512400	0.20187500
N	4.98438600	-0.19645100	0.27411200
N	-5.04911200	-0.42224100	0.17823000
P	-9.68032100	1.57788600	1.43914600
P	-9.84039200	-2.38332400	-0.13541800
P	9.46280800	1.90798800	-1.33069500
P	9.88843900	-1.70108200	1.14094400
C	9.83583600	3.60131000	-1.97054400
C	9.93512000	4.73756000	-1.15463000
C	10.02431400	3.74215800	-3.35243000
C	10.21092900	5.98530400	-1.71091200
H	9.79903100	4.63914400	-0.08270200
C	10.29140900	4.99246700	-3.91151200
H	9.96303700	2.86387300	-3.98929000
C	10.38656200	6.11599200	-3.09039300
H	10.28752500	6.85774600	-1.06852200
H	10.43275000	5.08739300	-4.98405500
H	10.60158200	7.08908900	-3.52173800
C	10.11261600	2.04626100	0.38989900
C	9.32676700	2.30604900	1.51854600
C	11.49036700	1.84521400	0.55862300
C	9.90326300	2.34937400	2.78810600
H	8.26100000	2.47205000	1.40565600
C	12.06844600	1.89858100	1.82465600
H	12.10809000	1.63510300	-0.30936100
C	11.27344200	2.14381500	2.94551500
H	9.27928900	2.54422000	3.65551700
H	13.13684300	1.73995300	1.93843100
H	11.71968600	2.17343100	3.93492100
C	10.57702300	-3.36182000	1.56994000

C	10.93392800	-3.58850700	2.90650400
C	10.75305400	-4.39478100	0.63794000
C	11.44179100	-4.82433100	3.30876600
H	10.81354400	-2.78883500	3.63228300
C	11.26929400	-5.62637500	1.03697300
H	10.48711100	-4.22870100	-0.40072100
C	11.61178700	-5.84489300	2.37323200
H	11.71164600	-4.98670600	4.34804700
H	11.40308300	-6.41796800	0.30544500
H	12.01392700	-6.80519000	2.68191700
C	10.32482800	-1.60315500	-0.64861600
C	11.62650700	-1.18180500	-0.95627900
C	9.44413800	-1.89078600	-1.69754300
C	12.03668400	-1.04582400	-2.28027100
H	12.31556300	-0.94820200	-0.14995600
C	9.85091300	-1.74498400	-3.02378600
H	8.43623200	-2.22581000	-1.47807500
C	11.14552100	-1.32008300	-3.31911000
H	13.04783500	-0.71723500	-2.50214000
H	9.15309200	-1.96303700	-3.82694100
H	11.45920800	-1.20252500	-4.35193500
C	-10.44512200	-3.97964700	-0.84745800
C	-10.67163300	-5.03308900	0.05102300
C	-10.68607700	-4.19340300	-2.21165100
C	-11.10825800	-6.27732600	-0.40317800
H	-10.50372400	-4.87327600	1.11272500
C	-11.13497900	-5.43345000	-2.66489500
H	-10.52479500	-3.38653700	-2.91814000
C	-11.34284900	-6.47899900	-1.76372600
H	-11.27406200	-7.08413500	0.30453300
H	-11.32076500	-5.58442300	-3.72434100
H	-11.69147800	-7.44390700	-2.11946300
C	-10.24896800	-1.19771400	-1.48600900
C	-9.42835500	-0.96883500	-2.59933400
C	-11.45884000	-0.49975900	-1.38222100
C	-9.81577100	-0.06777900	-3.58925400
H	-8.48437900	-1.49680300	-2.68709800
C	-11.85065000	0.39390300	-2.37728700
H	-12.08712600	-0.64799700	-0.50871600
C	-11.02893500	0.61318700	-3.48153100
H	-9.16842100	0.10612800	-4.44403500
H	-12.78326900	0.93855900	-2.27784100
H	-11.32398000	1.32581200	-4.24464500
C	-10.10256700	2.81745600	2.74496200
C	-10.36446000	2.31557500	4.02803200
C	-10.16677000	4.20393800	2.53817700
C	-10.66888200	3.17554900	5.08297900
H	-10.33221100	1.24254000	4.19605500
C	-10.48033500	5.06357200	3.59031300
H	-9.97433400	4.60794700	1.55026800
C	-10.72918100	4.55216400	4.86530900
H	-10.86751900	2.77061100	6.07077300
H	-10.52723000	6.13448900	3.41528000
H	-10.97377200	5.22324700	5.68316200
C	-10.06756200	2.53775500	-0.09168500
C	-9.14225900	2.74218600	-1.12111700
C	-11.37279500	3.03137300	-0.25362300
C	-9.50620800	3.43923200	-2.27383300
H	-8.13099400	2.36491600	-1.02159600
C	-11.72965400	3.74293400	-1.39585300
H	-12.10779500	2.87430000	0.53081400
C	-10.79512800	3.95066800	-2.41223900

H	-8.77440800	3.58754600	-3.06242100
H	-12.73878700	4.13255100	-1.49424600
H	-11.07220200	4.50247600	-3.30540800

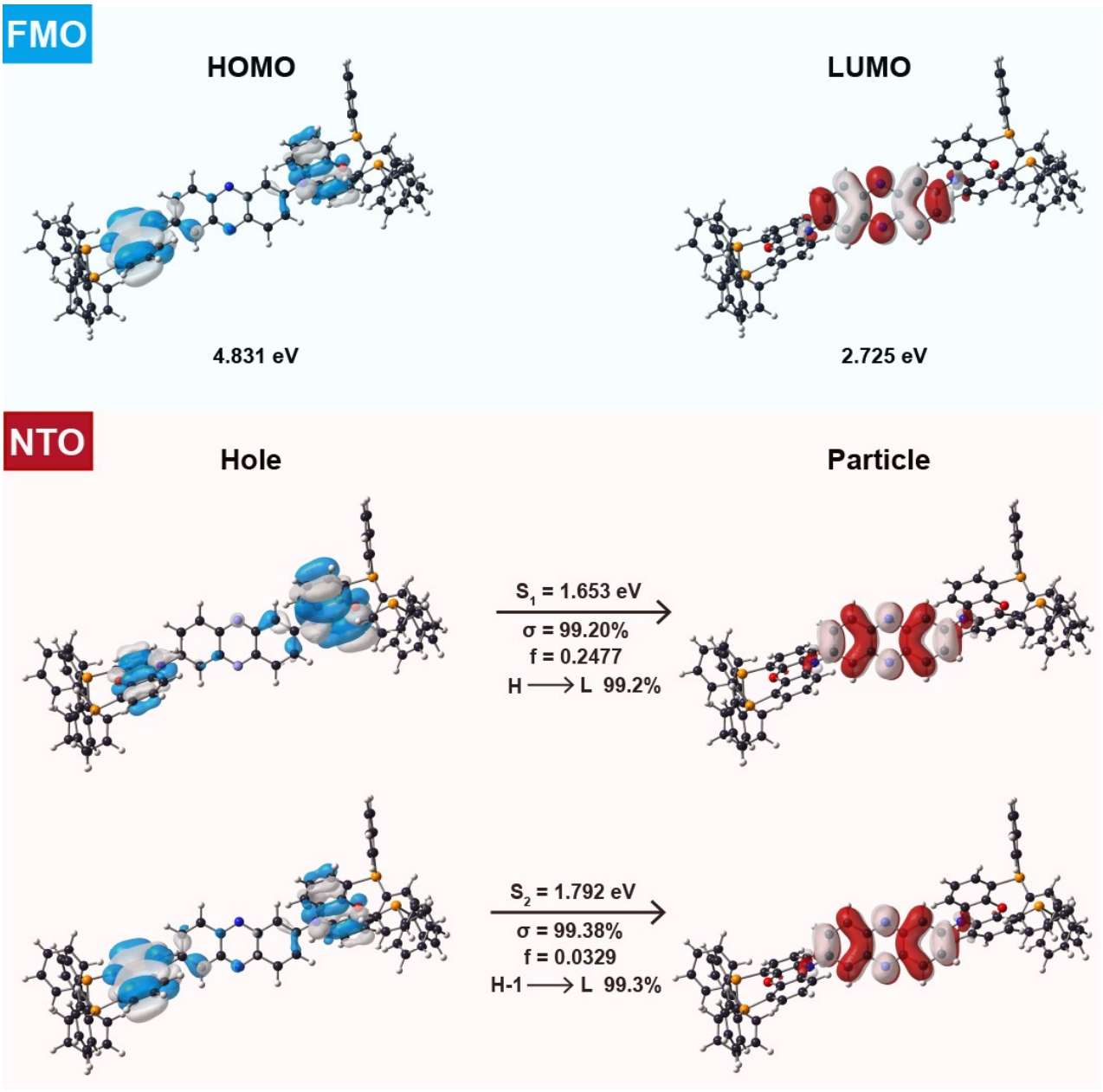

Figure S16. HOMO and LUMO for FMOs. Excited energy, oscillator strength (f), transition probability (σ) and orbital constitutes of NTO.

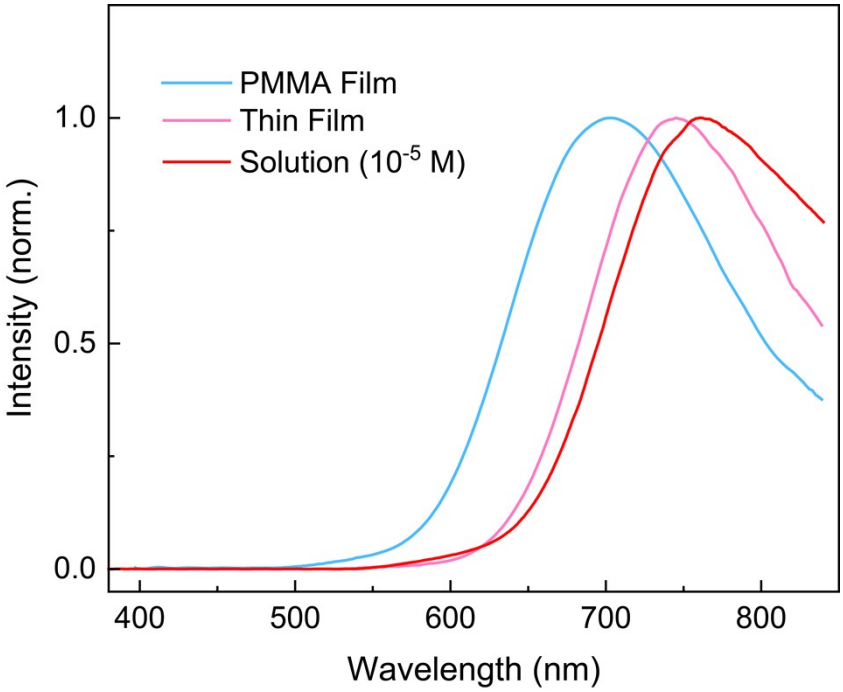

Figure S17. The emission spectra of DPh_2P-POZ-PZ in different matrixed.

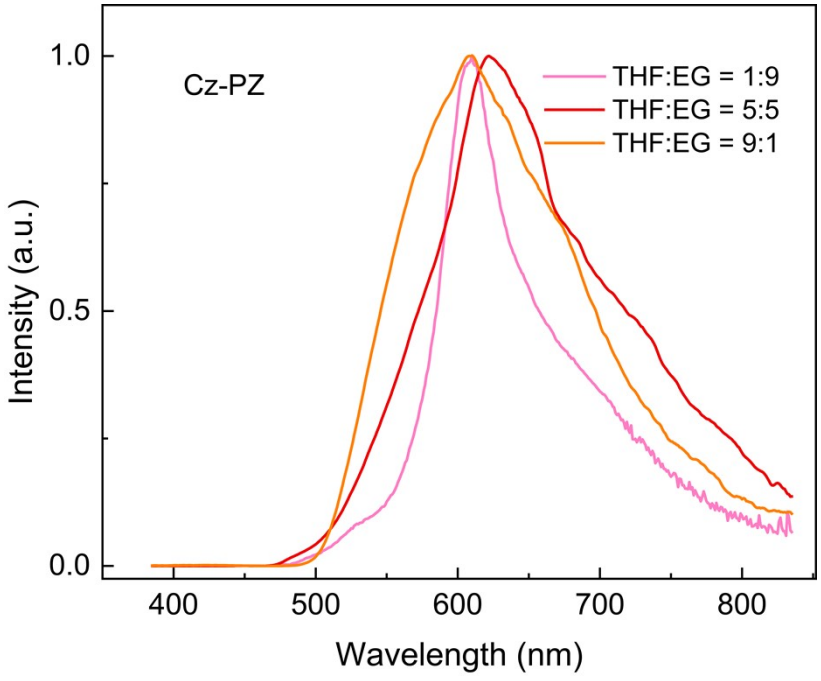

Figure S18. The emission spectra of Cz-PZ in different viscosity.

The Cz-PZ is also measured to verify the existence of self-vibration and rotation in different viscosity. As shown in figure S18, the emission spectra of Cz-PZ in different viscosity do not perform blue emission, which indicates that due to the feasible dihedral angle (43°), the electronic of Cz group could transfer to PZ group effectively rather than consuming via self-vibration of Cz. Therefore, there is no dual emission can be observed in different viscosity.

Figure S19. The emission picture of POZ-PZ in THF and liquid paraffin (LP) combination.

To mitigate the impact of polarity variation, we utilize liquid paraffin instead of ethylene glycol (although the polar effect of EG is also minimal), and the observed phenomena are identical. As illustrated in the image, the visible emission color shifts from deep blue to red as viscosity increases. It is important to note that the emission intensity of the high-viscosity combination is significantly higher than that of the low-viscosity combination. As stated in the manuscript, this enhanced intensity is attributed to the restrictive matrix. Therefore, the augmented intensity and variable color provide sufficient evidence that the molecular configuration is induced by the matrix

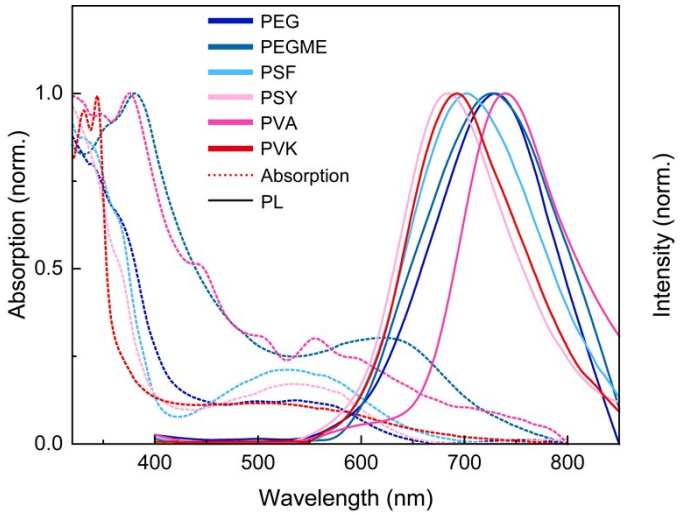

Figure S20. The emission spectra of POZ-PZ in various polymer. (5% w/w doped concentration in polyethylene glycol (PEG), Poly(ethylene glycol)methyl (PEGME), poly(vinyl alcohol) (PVA), polystyrene (PSY), polysulfone (PSF), polyvinylcarbazole (PVK), respectively)

As shown in Figure S20, the absorption and the emission spectra of POZ-PZ in different polymers reveal that the induced effects of different matrixes on the structure of POZ-PZ lead to distinct emission peaks. This result strongly supports our hypothesis. It is worth noting that PEGME and PEG have very similar structures, resulting in their highest emission peaks nearly overlapping. However, due to the presence of methyl groups in PEGME, there is a slight difference in the width of the emission peak, which further confirms our conjecture about matrix-induced effects.

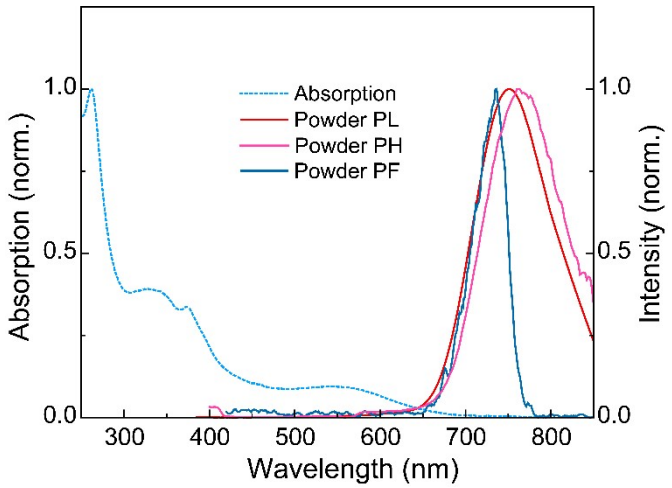

Figure S21. The absorption, photoluminescence (PL), prompt fluorescence (PF), phosphorescence (PH) of POZ-PZ in powder state.

As shown in Figure S21, we conducted optical property tests on the POZ-PZ in its powder state. The photoluminescence (PL) emission wavelength of the POZ-PZ in the powder state is approximately 752 nm, which is similar to the emission wavelength in the film state. The prompt fluorescence (PF) and phosphorescence (PH) emissions are observed at approximately 735 nm and 762 nm, respectively. The energy difference between the PF and PH emission peaks, denoted as ΔE_{ST}, is approximately 0.06 eV. Furthermore, comparing the emission in the powder state to that in the solution state, it is found that the blue emission is completely absent. Additionally, the emission peaks are very close to those observed in the film state, suggesting a close similarity between the molecular structures of the compound in the powder and film states.

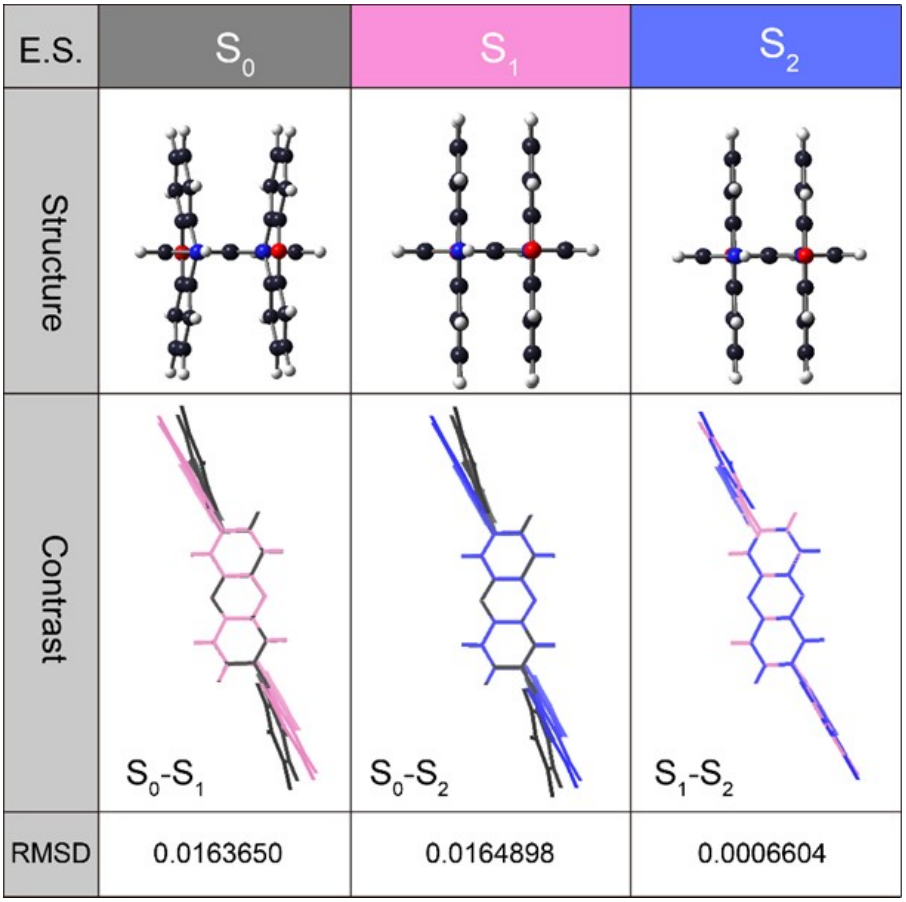

Figure S22. The contrast diagram of different excited state conformation in solution state.

As mentioned in manuscript, the dihedral angle between POZ and PZ is vertical in solution state, which results in the blue emission raised from self-vibration of POZ group. For further proving this, the molecule conformations of S_1 and S_2 are optimized. The structures are arranged as following:

By comparing the molecular conformations in different excited states (Figure S22), it can be observed that the PZ moiety undergoes little noticeable structural change. Although the POZ group is vertical to the PZ in all excited states, it undergoes more pronounced changes. In the S_0 state, the POZ group exhibits slight bending, while in the S_1 and S_2 states, the POZ becomes completely planar. To visualize the structural changes between S_0 and S_1, S_0 and S_2, as well as S_1 and S_2, we introduced **RMSD** (Root Mean Square Deviation) to quantify the molecular variations.

$$RMSD = \sqrt{\frac{1}{N}\sum_{i}^{natom}[(x_i - x_i^{'})^2 + (y_i - y_i^{'})^2 + (z_i - z_i^{'})^2]}$$

In the equation, "i" iterates over all atoms, where x_i and x_i' represent the x-coordinate of the i th atom in the first and second structures, respectively. The same applies to the y and z coordinates.

Since the PZ group undergoes minimal changes, we can use it as a reference coordinate to compare the molecular variations. According to the RMSD, the structure changes of S_0-S_1 and S_0-S_2 are very large, which are 0.0163650 and 0.0164898, respectively. The structure change of S_1-S_2 is only 0.0006604. This indicates that in the excited state, the molecule experiences changes only in the POZ group, while the dihedral angle remains at 90°. This implies that the electronic transfer from the POZ group to the PZ group remains inefficient, leading to the absence of CT emission. Additionally, the TD-DFT calculations for different structures also support our hypothesis. They show that both S_1 and S_2 structures have an oscillator strength of 0, indicating no emission, while only the S_3 excited state exhibits emission. This aligns with our proposed conjecture that in the dual-emission phenomenon, the blue emission originates from the S_2 excited state in the ground-state structure, while the red emission arises from the CT transition occurring when the dihedral angle is less than 90°.

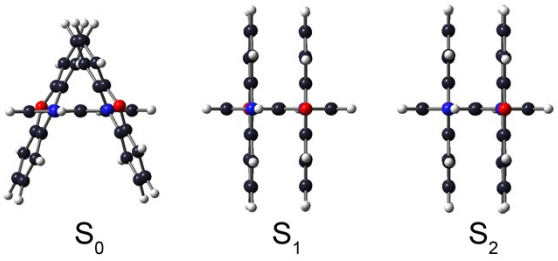

Figure S23. The contrast diagram of different excited statae.in thin film

As shown in Figure S23, in the thin film state, the dihedral angle between the POZ group and the pz group in the ground state structure is approximately 68.9°. However, without any restrictive optimization, both S_1 and S_2 exhibit an angle of 90°. This indicates that molecules in the thin film state tend to twist upon excitation. However, it is undeniable that in the thin film state, the molecular conformation is induced by the rigid matrix and cannot realize twisting. Furthermore, TD-DFT calculations for the S_1 and S_2 conformations reveal transition wavelengths that do not match the experimental data, while only the TD-DFT calculation for the ground state structure align with the experimental results. This suggests that the simulated ground state molecular structure is the most similar with the real structure in the thin film state. Meanwhile, it also indicates that in the thin film state, the molecule adapts to the matrix-induced conformation and exhibits photophysical properties which specific to that conformation.

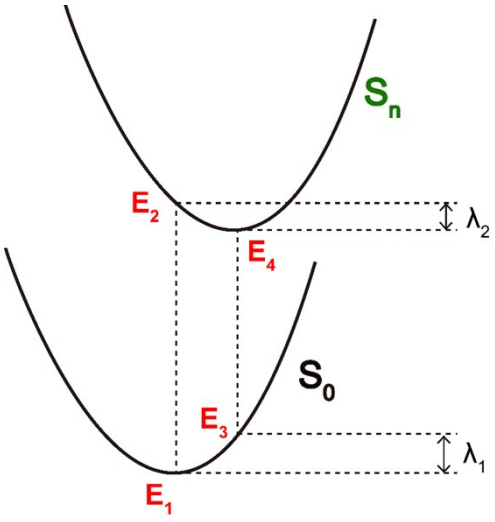

Figure S24. The contrast diagram of different excited statae.in thin film

As shown in Figure S24, λ is the reorganization energy, where λ_1 should be approximate to λ_2 if the molecule conformation obtains an appropriate optimization:

Table S5. The reorganization energies of diverse excited state.

Solution State	λ1	λ2	Film State	λ1	λ2
S_0-S_1	3.10 kcal/mol	3.10 kcal/mol	S_0-S_1	4.86 kcal/mol	4.86kcal/mol
S_0-S_2	3.13 kcal/mol	3.13 kcal/mol	S_0-S_2	4.87kcal/mol	4.87 kcal/mol

From the table S5, it can be observed that in the solution state, the reorganization energy corresponding to the structural relaxation after the vertical transition from the S_0 equilibrium structure to S_1 is 3.10 kcal/mol, which is equal to the reorganization energy of 3.10 kcal/mol associated with the structural relaxation upon returning vertically from S_1 to S_0. Similarly, when the S_0 equilibrium structure vertically transitions to S_2, the reorganization energy corresponding to the structural relaxation is 3.13 kcal/mol, which is comparable to the reorganization energy generated from S_0 to S_1. This indicates that the potential energy surface curvature is same in the direction between the S_0-S_1 minimum structure and the S_0-S_2 minimum structure, as the energy change λ is the same for the S_0-S_1 and S_0-S_2 transitions when displaced in the same manner. Considering that the oscillator strength of the S_1 structure in the ground state is zero, while the exciton strength of the S_2 excited state is non-zero, the exciton will experience de-excitation in the S_2 excited state. This result is consistent with experimental observations. Similarly, when calculating the thin film state, the reorganization energy for S_0-S_1 and S_0-S_2 is almost identical, and the oscillator strength of S_1 in the ground state is much larger than that of S_2. Therefore, the compound only exhibits near-infrared emission in a rigid matrix.

References

[1] T. Nakagawa, S. Y. Ku, K. T. Wong, C. Adachi, Electroluminescence based on thermally activated delayed fluorescence generated by a spirobifluorene donor–acceptor structure, *Chem. Commun.* 2012, **48**, 9580-9582.
[2] M. Frisch, G. Trucks, H. Schlegel, G. Scuseria, M. Robb, J. Cheeseman, J. Montgomery, J. Vreyen, K. Kudin, J. Burant, J. Millam, S. Iyengar, J. Tomasi, V. Barone, B. Mennucci, M. Cossi, G.Scalmani, N. Rega, G. Petersson, H. Nakatsuji, M. Hada, M. Ehara, K. Toyota, R. Fukuda, J. Hasegawa, M. Ishida, T. Nakajima, Y. Honda, O. Kitao, H. Nakai, M. Klene, X. Li, J. E. Knox, H. P. Hratchian, J. B. Cross, C. Adamo, J. Jaramillo, R. Gomperts, R. Stratmann, O. Yazyev, A. Austin, R. Cammi, C. Pomelli, J. Octhterski, P. Ayala, K. Morokuma, G. Voth, P. Salvador, J. J. Dannenberg, V. G. Zakrzewski, S. Dapprich, A. D. Daniels, M. C. Strain, O. Farkas, D. K. Malick, A. D. Rabuck, K. Raghavachari, J. Foresman, J. V. Ortiz, Q. Cui, A. G. Baboul, S. Clifford, J. Cioslowski, B. Stefanov, A. L. G. Liu, P. Piskorz, I. Komaromi, R. L.Martin, D. J. Fox, T. Keith, M. A. Al-Laham, C. Y. Peng, A. Nanayakkara, M. Challacombe, P. M. W. Gill, B. Johnson, W. Chen, M. W. Wong, C. Gonzalez, J. A. Pople, Gaussian 03, Revision D.02, Gaussian Inc., Pittsburgh, PA 2004.
[3] T. Lu, F. Chen, Multiwfn: A multifunctional wavefunction analyzer, *Comput. Chem*. 2012, **33**, 580-592.
[4] Z. Yang, Z. Mao, C. Xu, X. Chen, J. Zhao, Z. Yang, Y. Zhang, W. Wu, S. Jiao, Y. Liu, M. P. Aldred, Z. Chi, A sterically hindered asymmetric D–A–D′ thermally activated delayed fluorescence emitter for highly efficient non-doped organic light-emitting diodes, *Chem. Sci*. 2019,**10**, 8129-8134.
[5] M. Xie, J. Cai, X. Wang, T. Shan, S. Jung, H. Zhong, X. Guo, D. Zhou, T. Li, Simple phenazine-based compounds realizing superior multicolored emission, *Adv. Opt. Mat.* 2022, **10**, 2102443.